Journal of Engg. Research Vol.10 No. (4B) pp. 199-215 DOI: 10.36909/jer.10569

Experimental and numerical analysis of flow characteristics of sand-water slurry in a horizontal pipe

Varinder Singh*, Satish Kumar and Dwarikanath Ratha*****

** Mechanical Engineering Department, Thapar Institute of Engineering and Technology, Patiala, 147004, India*
*** Mechanical Engineering Department, National Institution of Technology, Jamshedpur, Jharkhand 831014, India*
**** Civil Engineering Department, Thapar Institute of Engineering and Technology, Patiala, 147004, India*
*** Corresponding Author: satish.me@nitjsr.ac.in*

Submitted *:* 16/05/2020
Revised *:* 12/08/2021
Accepted *:* 23/08/2021

ABSTRACT

The transportation of the solid material using hydraulic transportation method is economically the best method. The head loss occurs during transportation of slurry through horizontal pipelines and usually depends on the rheological behavior of slurry, slurry concentration, particle size, and influx velocity. An experimental investigation has been performed using sand-water slurry flowing through the horizontal pipe section of a pilot plant test loop. The head loss obtained from the experimental results was validated through CFD simulation using FLUENT. The solid concentration of sand-water slurry and influx velocity used during both experiments and numerical simulation were in the range of 10–40% (by weight) and 1 to 4 m/s, respectively. The numerical simulations were performed using five different turbulence models, and the results obtained using SST k-omega model were in close agreement with experimental results. It is observed from both the experiment and numerical analyses that the pressure loss, granular pressure, volume fraction, and skin fraction coefficient during transportation of slurry through a horizontal pipe are functions of solid concentration and influx velocity. The present study observed that as the flow velocity increases four times, the pressure loss is increasing more than 10 times. Uniform volume fraction at middle zone of outlet of the pipe is observed as both the slurry concentration and velocity of flow increase.

Keywords: Volume fraction; Pressure loss; SST k-omega model; Granular pressure.

NOMENCLATURE

∇P	Static pressure loss	$\bar{\bar{\tau}}_W$	Water Phase viscous stress tensor
ρ_{SA}	Density of sand particles phase (kg/m^3)	$\bar{\bar{\tau}}_{SA}$	Sand particle Phase viscous stress tensor
W	Water phase	φ	internal friction angle

$a_{SA,max}$	slurry settling concentration	$\bar{\bar{\tau}}_{t,SA}$	Reynolds stress tensor for sand particles phase
SA	Sand particle phase	C_L	Lift force coefficient
m_{SA}	Sand Particle mass flow rate in kg/sec	$\vec{g}$	Acceleration due to gravity
$\nabla\bar{\bar{\tau}}_W$	Viscous force for water phase	$\bar{\bar{\tau}}_{t,W}$	Reynolds stress tensor for fluid
G_{kin}	generation of kinetic energy	Γ_ω	diffusivities of ω
∇P_{SA}	Sand particles pressure loss	C_{vm}	Virtual mass force coefficient
d_{SA}	Sand particle diameter	$\nabla\bar{\bar{\tau}}_{SA}$	Viscous force for sand particles phase.

INTRODUCTION

The transportation of the solid material using hydraulic transportation method is, technically and economically, the best method. This method is commonly used in many industries like food processing, chemical industry, mining industry, and mineral industry. This transportation method has been also used in tailings, coal ash disposal operations, and bulk material transportation. The hydraulic transportation system is an environmentally-friendly process as this process has mostly no adverse impacts on environment (Aude et al., 1975). The main beneficial features of the hydraulic transportation system are as follows: easy installation process, less space requirement, efficient, reliable, easy operation, long working life, less storage cost, easy automation, less human resources required, low maintenance, easily crossing every type of obstacles (rivers, railways tracks, and roads), less chance of any types of accident, less noise, and low energy consumption. The pipe transitions present during hydraulic transportation system create serious problems like pressure drop, slurry settling, power conception, influx velocity, granular pressure, choking, blockage, back pressure, etc. These flow-related problems usually depend on various design parameters such as diameter of the pipe, solid concentration, type of the pump, and distance between the transportation stations. But designing of such a transportation system requires huge experimental data. Also, great efforts are required to identify efficient slurry pumps, which can minimize the consumption of power (Singh et al., 2019).

The literature review shows that most of the researchers determined the flow characteristics of slurry through pipes for low solid concentrations experimentally and further developed an empirical relation between solid concentration and flow velocity (Yang et al., 2019; Liu et al., 2009; Lin & Ebadian 2008; Ling et al., 2003; Ghanta & Purohit, 1999; Sundqvist et al., 1996, Liao et al., 2020). Analysis of the flow problems through only experimentation is a very complex method and time consuming. Therefore, researchers use computational techniques as the cost of computation method using CFD is less in comparison to the generation of data through experiments. In the CFD tool, the governing equations of slurry flowing through pipes are solved by using a numerical algorithm on a powerful computer system. Because of the complex system, many trials are usually made for simulations of slurry flowing in the pipeline. Ling et al. (2003) investigated the sand-water slurry flowing in a horizontal pipeline using an algebraic slip mixture model of CFD and validated the simulation results with experimental results. Lin and Ebadian (2008) used the ASM model to investigate the numerical solution of sand-water slurry flowing in the entrance part

of the straight pipeline. Vlasak et al. (2020) conducted an experimental study of sand slurry up to 35% concentration flowing through a 100 mm pipe diameter and concluded that the pipe inclination, slurry concentration, and mean velocity affect the flow characteristics.

The main aim of the present work is to explore the abilities of computational fluid dynamic tools to model such types of complicated flow problems in the horizontal pipe section. It is found from the literature review that most of the experimental works on sand slurry flow through a horizontal pipeline are limited to 30% slurry concentration (Archibong-Eso et al., 2020; Dabrian et al., 2018; Gopaliya and Kaushal, 2015), whereas very few works are available on determination of flow characteristics during the flow of sand-water slurry having a concentration equal to or greater than 35% (Vlasak et al., 2020, Ahmed et al., 2018). Most of the studies carried out for higher sand-water slurry concentrations are based on numerical simulation. But limited experimental studies are available on sand-water slurry at higher concentrations along with varying influx velocity. In most of the studies, the researchers have validated their results with experimentation using a single CFD model. In the present study, the sand-water slurry of particle size of 150–106 μm with solid concentrations of 10–40% at the slurry influx velocity of 1–4 m/s has been used for experimentation, and the flow characteristics for different conditions have been analyzed numerically.

EXPERIMENTATION

The experiments were performed on a pilot plant test loop, which is available at Thapar Institute of Engineering and Technology. Sand slurry was made to flow through this test loop, and pressure head loss was determined at required points. Figure 1 shows the schematic diagram of the pilot plant test loop for slurry transportation. This pilot plant test loop consists of a 60-meter-long pipeline of 100 mm in diameter. It consists of two trapezoidal shape containers, one for slurry preparation and the other for water storing. The water storing container was used for cleaning the slurry pipeline after performing the experiment. In order to ensure the uniform mixing of slurry and to avoid the settling of sand particles in slurry preparation containers, a gearbox stirrer (reduction ratio 1:30) was provided at the top of the container. A stirrer consists of rectangular plates was welded around the periphery of a 30 mm pipe. A progressive cavity slurry pump (Make by SYNO Engineer Ltd. with model no. SDA4 S17000 CWWTRG, Kanpur) was used to transport the sand-water slurry through test loop. The specification of the progressive cavity slurry pump is mentioned in Table 1.

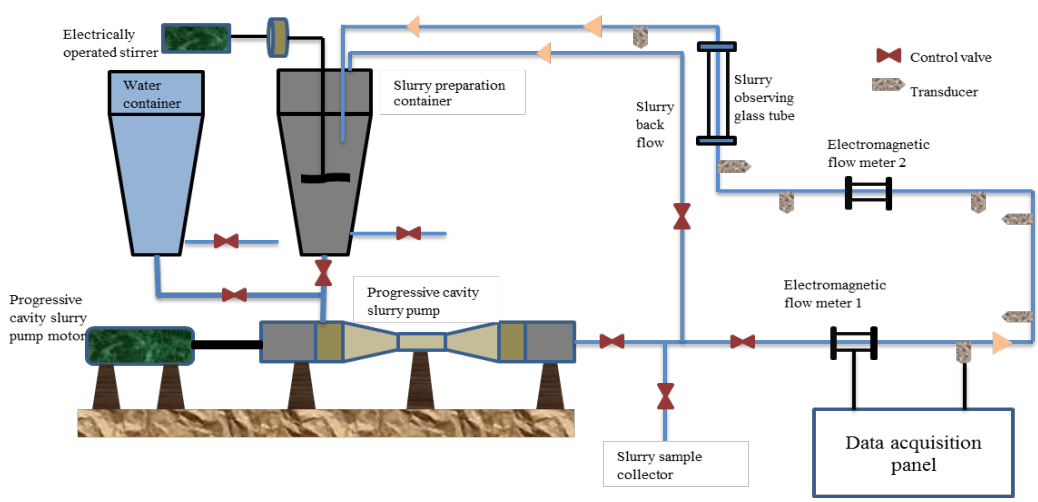

Figure 1. Schematic diagram of the pilot plant test loop.

Table 1. Specification of progressive cavity slurry pump.

Parameters	Values
pH value	5–7.7
Power required	11.1Kw
Temperature	Up to 80oC
Revelation per minutes	360
Maximum flow rate	60 m^3/h

The operating velocity of the pump is controlled by manually operative virtual frequency drive. A data acquisition system with data logger having 16 inputs ports was used for storing the data generated during experiments. The electromagnetic flow meter (make by Iota flow system with model no. MM-50-1STS-TP68-2MP, India) was used to measure the flow rate of slurry. The Flush type transducers (Make by WIKA Alevander Wiegand SE and Co. with model no. S11, Germany) were used to measure the pressure generated at various locations in the pipe. The experiments were performed to measure the pressure loss during the transportation of sand-water slurry in the horizontal pipeline having concentration range varying from 10 to 40%. The experiments were carried out for different velocity of the flow ranging from 1 to 4 m/s. The pressure loss in the slurry pipeline was measured in terms of Pascal per meter of the slurry pipeline.

NUMERICAL SIMULATION

The CFD simulation was performed by using the Navier–Stokes equations and Eulerian-multiphase model through FLUENT software. The results obtained from numerical simulations were validated with experimental results. The Eulerian model is generally used for multiphase flow, in which the volume fraction of each phase is assumed to be a continuous function of space and time. So, the sum of the volume concentrations of fluid and solid is equal to 1.0. The granular kinetic theory was used in the Eulerian mathematical model in order to define the interface between slurry particles. The first-order governing equations, that is, conservation of mass, energy, and momentum, were solved separately for every step. In this simulation, water is considered as a fluid phase (primary phase), and sand particle is considered as a solid phase (secondary phase). The fluid phase is denoted by (W), and solid phase indicated by (SA). The concentration of the fluid (primary) and solid (secondary) phases was represented as α_W and α_{SA}.

GOVERNING EQUATIONS

Eq. 1 represents the continuity equation based on conservation of mass for solid sand particle phase, which is used to evaluate the volumetric fraction of solid phase (SA) and fluid phase (W).

$$\frac{\partial}{\partial t}(a_{SA}\rho_{SA}) + \nabla(a_W\rho_W v_W) = \sum_{SA=1}^{n}(m_{SAW} - m_{WSA}) + S_{SA} \quad (1)$$

Eq. 2 and 3 represent the momentum equation for fluid phase and sand particle phase, respectively.

$$\nabla(a_W\rho_W\vec{V}_W\vec{V}_W) = -a_W\nabla P + \nabla\cdot\left(\bar{\bar{\tau}}_W + \bar{\bar{\tau}}_{t,W}\right) + K_{SAW}(\vec{V}_{SA} - \vec{V}_W) + C_{vm}a_{SA}\rho_W\left(\vec{V}_{SA}\cdot\nabla\vec{V}_{SA} - \vec{V}_W\cdot\nabla\vec{V}_W\right) + C_L a_{SA}\rho_W\left(\vec{V}_W - \vec{V}_{SA}\right)\times\left(\nabla\cdot\vec{V}_W\right) + a_W\rho_W\vec{g} \quad (2)$$

$$\nabla(a_{SA}\rho_{SA}\vec{V}_{SA}\vec{V}_{SA}) = -a_{SA}\nabla P - \nabla P_{SA} + \nabla\cdot\left(\bar{\bar{\tau}}_{SA} + \bar{\bar{\tau}}_{t,W}\right) + K_{WSA}(\vec{V}_W - \vec{V}_{SA}) + C_{vm}a_{SA}\rho_W\left(\vec{V}_W\cdot\nabla\vec{V}_W - \vec{V}_{SA}\cdot\nabla\vec{V}_{SA}\right) + C_L a_{SA}\rho_W\left(\vec{V}_{SA} - \vec{V}_W\right)\times\left(\nabla\cdot\vec{V}_W\right) + a_{SA}\rho_{SA}\vec{g} \quad (3)$$

When sand particles velocity becomes zero, then the correlation terminal velocity is achieved. It is the lowest flow velocity at which slurry can flow in the pipe without settling.

K-ω Turbulence Model

The SST k-omega model, a computational fluid dynamics turbulence model, was developed by Menter (1994) after using the solution of k-ω and k-ε models for slurry flowing in the pipeline. The SST model means shear stress transportation model, and k-ω means the eddy viscous model. The standard SST models exhibit less sensitivity to flow outside the boundary layer than many other CFD turbulence models (Menter, 1994). The k-ω model is the best model for simulating flow in the viscous sublayer. In the turbulence equation, the k variable is denoted as turbulence kinetic energy (kin), and ω variable is denoted as the specific rate of dissipation. The turbulence equations for the slurry pipeline are given in equations 4 and 5:

$$\rho\left(\frac{\partial kin}{\partial t} + \frac{\partial}{\partial x_a}\left(kinu_a\right)\right) = \frac{\partial}{\partial x_b}\left(\Gamma_{kin}\frac{\partial V}{\partial x_b}\right) + G_{kin} - Y_{kin} + S_{kin} \quad (4)$$

$$\rho\left(\frac{\partial \omega}{\partial t} + \frac{\partial}{\partial x_b}\left(\omega u_b\right)\right) = \frac{\partial}{\partial x_b}\left(\Gamma_{\omega}\frac{\partial \omega}{\partial x_b}\right) + G_{\omega} - Y_{\omega} + S_{\omega} + D_{\omega} \quad (5)$$

Geometry Detail and Meshing

Figure 2 shows the geometry of the horizontal pipeline. The total length of the pipe is 2000 mm with an internal diameter of 100 mm. The length of the pipe in the present study was decided in such a way that it will ensure the fully established flow within the domain.

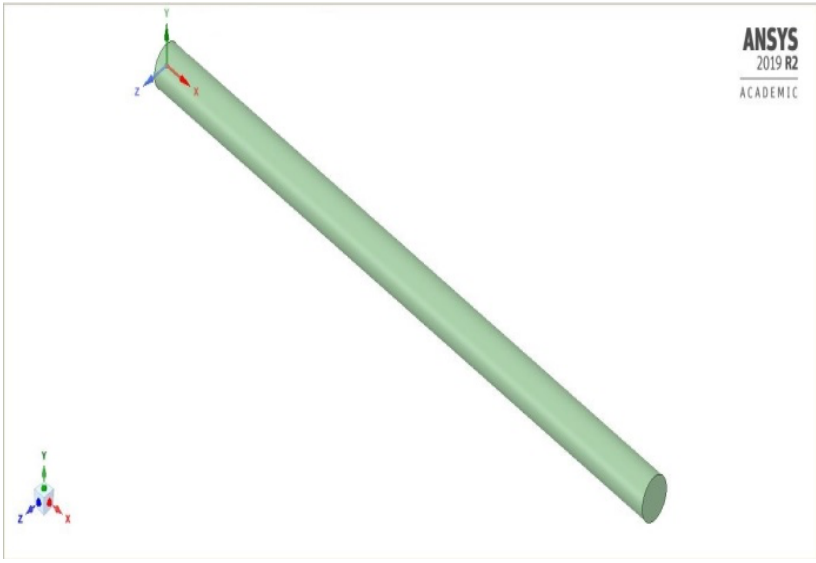

Figure 2. Geometry of straight and horizontal pipeline.

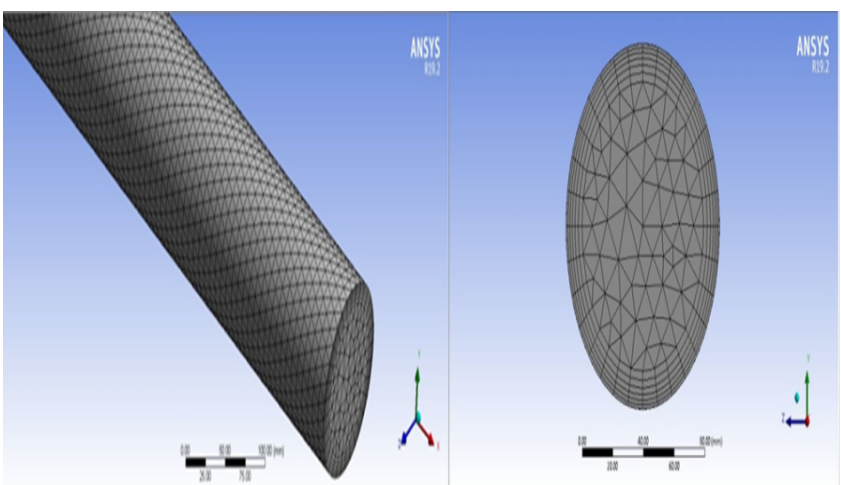

Figure 3. Meshing structure of straight and horizontal pipeline.

The present study used the tetrahedral type elements for the meshing of the pipeline. The distribution of the mesh on the circumference of the pipeline was uniform, which is shown in Figure 3. The inflation has been applied at the boundary of the pipe for the refinement of a mesh. The boundary of the mesh was refined by taking the growth rate of 1.2. In order to refine the mesh of the pipe, 6 inflation layers of size 0.272 are used. The mesh independence tests were carried out to optimize the number of cells in the pipe geometry. The value of the y+ near to wall is found as 102.74. The y+ value of straight pipe is the dimensionless pipe wall distance for the adjacent cell to the pipe wall. The details of mesh quality for different mesh sizes are given in Table 2. It is found that the orthogonal quality, skewness, and aspect ratio for various mesh sizes are lying in the range of 0.82–0.84, 0.15–0.18, and 3.6–4.25, respectively. Since all the values are lying within the permissible limits, it indicates that the mesh is of good quality.

Table 2. Details of mesh quality.

Mesh size (mm)	8	9	10	11	12
Skewness	0.1622	0.1585	0.1674	0.1679	0.1787
Orthogonal quality	0.8368	0.8406	0.8319	0.8315	0.8208
Aspect Ratio	3.6389	3.7795	3.9624	4.0845	4.2423
Element quality	0.6311	0.6137	0.5927	0.5775	0.5604

Boundary Conditions

Three surfaces are bounding the flow domain, namely, the inlet surface, the outlet surface, and the pipe wall surface. The inlet boundary condition was used to introduce the flow of sand-water slurry at a constant volume fraction and velocity. The slurry flow velocity at the inlet boundary section of the straight pipe was assumed as uniform in the whole length of the pipe. During the flow of slurry, the sand particles of slurry are assumed to be distributed uniformly in the pipeline. The no-slip condition was considered at pipe wall for liquid phase, and the pipe roughness constant was kept at 0.5. Tables 3 and 4 show the various input parameters and boundary conditions used in the present simulation.

Table 3. Input parameter used in simulation.

Fluid phase		Solid phase	
Fluid	Water	Solid	Sand
Density	1000 kg/m^3	Density	2650 kg/m^3
Influx velocity	1 to 4 m/s	Particle size	150–106µm
Pipe material	Mild steel	Solid concentration	10 to 40% (by weight)
Density	7850 kg/m^3	Influx velocity	1 to 4 m/s

Table 4. Boundary conditions.

Boundary	Inlet	Outlet	Wall
Boundary type	Velocity inlet	Pressure outlet	Wall
Velocity	Variable; 1–4 m/s	Not to be specified	0 m/s, due to no slip condition
Pressure	Operating pressure of 101325 Pa	Operating pressure of 101325 Pa	Operating pressure of 101325 Pa
Turbulence (medium intensity)	Specified as Turbulence intensity of 5%, and turbulent viscosity ratio 10	Specified as Turbulence intensity of 5%, and turbulent viscosity ratio 10	Not to be specified
Volume fraction	Variable; 0.0402–0.20100	Variable; 0.0402–0.20100	Not to be specified
Roughness constant	Not to be specified	Not to be specified	0.5

A first-order scheme was used to solve the turbulence kinetic energy, head loss correction, turbulence dissipation rate, and momentum equation. For the fast converging of simulation, the relaxation factors, that is, kinetic energy, momentum, pressure, body forces, and specific dissipation rate, were considered as 0.8, 0.7, 0.3, 1, and 0.8, respectively. Converging criteria of 10^{-3} were used for converging the numerical simulation. SIMPLEX algorithm along with the 3D segregated solver was used to solve the governing equation. All CFD simulations were performed on Intel Xenon E51607-v2, a Windows®10 based machine having a 16GB of RAM.

Grid Independency Test

In order to optimize the number of cells in the solution domain, the grid independency tests were carried out for six different mesh sizes. The flow domain was discretized into 8, 9, 10, 11, 12, and 13 mm mesh size, which created 329056, 236705, 180045, 140143, 112975, and 91715 numbers of elements, respectively. The grid independency tests were performed at 40% solid concentration with 4 m/s influx velocity. The average particle sand size of 150–106 μm was used for this simulation.

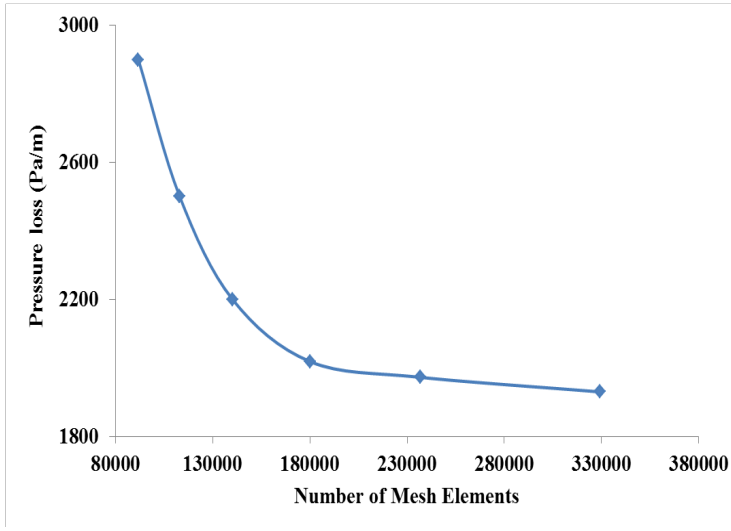

Figure 4. Grid independence test.

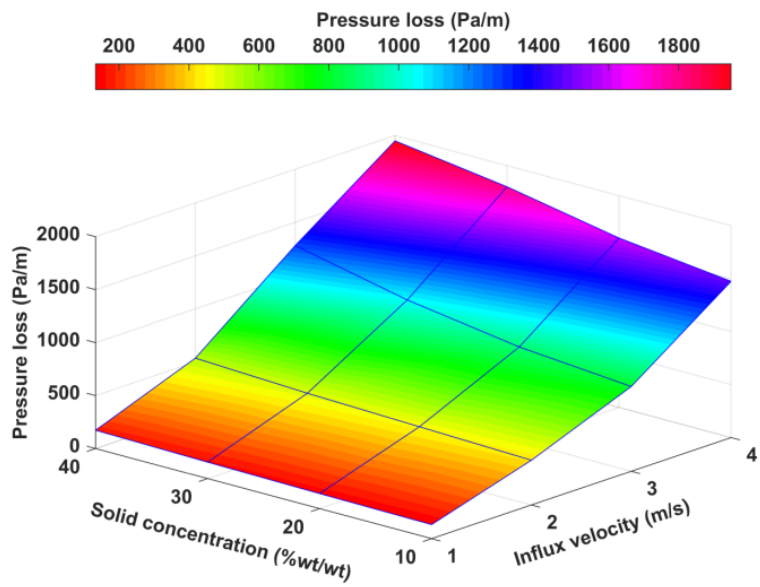

Figure 5. Pressure loss variations in pilot plant test loop.

The variation of the magnitude of pressure loss with the increase in mesh size was analyzed, which is shown in Figure 4. It is observed that there is an appreciable change in magnitude of the pressure loss with respect to increase in the number of elements from 91715 to 180045, and there is a negligible change in pressure loss when the number of elements increases beyond 180045. Therefore, the present study adopted the size of element 10 mm for meshing in the flow domain for all the simulations.

RESULTS AND DISCUSSIONS

The governing equations were solved within the flow domain using all the boundary conditions presented in Table 4 and four different turbulence models. In order to check the accuracy of the result, the present study considered the SST k-omega model, standard k-ε, realizable k-ε, and standard k-ω turbulence models for the simulations, and the results were compared with numerical simulation results in the published literature as well as the experimental study. Further, the results were interpreted with various flow characteristics, which are useful for the designing of the slurry pipeline.

Pressure Loss in Pilot Plant Test Loop

The pressure loss in the present study was measured in terms of Pascal per meter. The combined effect of solid concentration and influx velocity of the sand slurry on the pressure loss using the pilot plant test loop setup is shown in Figure 5. The solid concentration and influx velocity of the slurry were varying in the range of 10–40% (by weight) and 1–4 m/s, respectively. it is observed that the pressure loss in the pipeline increases with increasing influx velocity, keeping other flow parameters constant. The higher rate of enhancement of pressure loss is observed at 4m/s influx velocity for all range of slurry concentrations. Similarly, it is also noticed that the higher rate of enhancement of pressure loss is observed at 40% solid concentration for all range influx velocity. For influx velocity 1m/s, the value of pressure loss is observed as 133, 142, 155, and 172.5 Pa/m with a solid concentration of 10, 20, 30, and 40% (by weight), respectively. Similarly, for influx velocity 4 m/s, the value of pressure loss is observed as 1475, 1600, 1800, and 1950 Pa/m, respectively. Similar trends of pressure loss have also been presented by many investigators (Archibong-Eso et al., 2020, Yang et al., 2019).

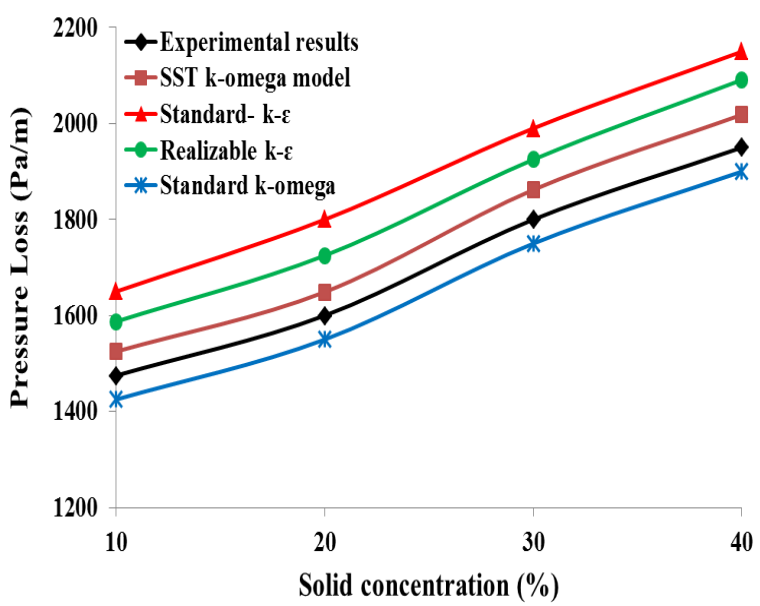

Figure 6. Pressure loss variations with different solid concentration at 4 m/s influx velocity.

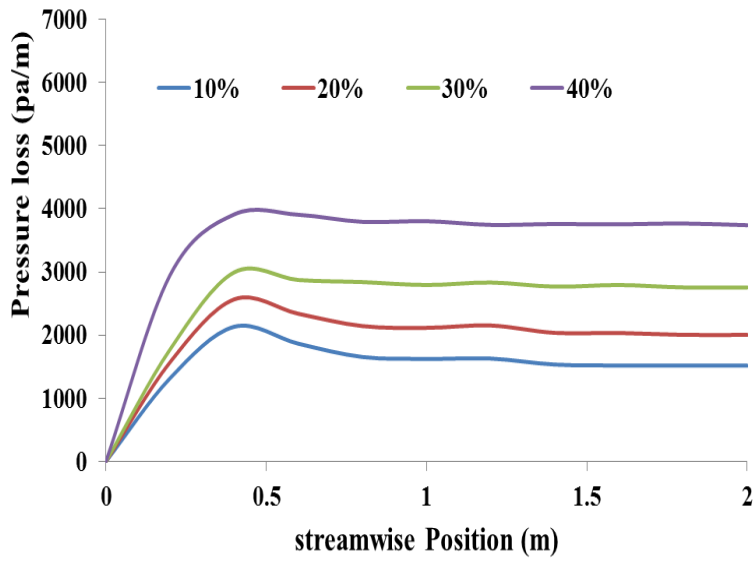

Figure 7. Pressure loss variations in the pipe for 10–40% solid concentration at 4 m/s influx velocity.

Pressure Loss in Numerical Simulation and Validation

The pressure loss during sand slurry transportation through a horizontal pipe was also determined through CFD using governing equations (1–3) using various turbulence models (Eq. 4-5) and boundary conditions represented in Table 4. The results obtained using numerical simulations were compared with the experimental results obtained through test loop. Figure 6 shows the variation of average pressure loss with all four solid concentrations at influx velocity of 4 m/s obtained by both experimentally and numerically. The increase in average pressure loss with increase in solid concentration is obtained from both experimental and numerical simulations, which can be seen from Figure 6. It is also observed that the pressure loss obtained using standard k-ω turbulence models is underpredicting, whereas SST k-omega, standard k-ε, and realizable k-ε turbulence model are overpredicting in comparison to experimental results. The deviation between experimental results and results obtained by the SST k-omega, Standard k-ε, Realizable k-ε, and Standard k-omega turbulence models at 40% solid concentration is 3.39, 9.30, 6.74, and -2.63%, respectively. Since the SST k-omega model established a close agreement with experimental results with a 3.39% maximum deviation in results, it was used for further analysis through numerical simulation. Adanez et al. (1993) measured pressure gradient for sand sizes 630–830 and 60–300 μm for different velocities and observed a pressure drop in a range of 0–450 kg/m^3 for different solid circulation flux at a gas velocity 3 m/s. The present study also obtained a pressure drop of 899–1356 Pa/m (91–139 kg/m^3) numerically for a slurry concentration range of 10–40% at a velocity 3 m/s having mean particle size 134μm. The pressure drops obtained through CFD in the present study are lying within the value obtained by Adanez et al. (1993), and the deviation in the magnitude is due to different particle size and concentration.

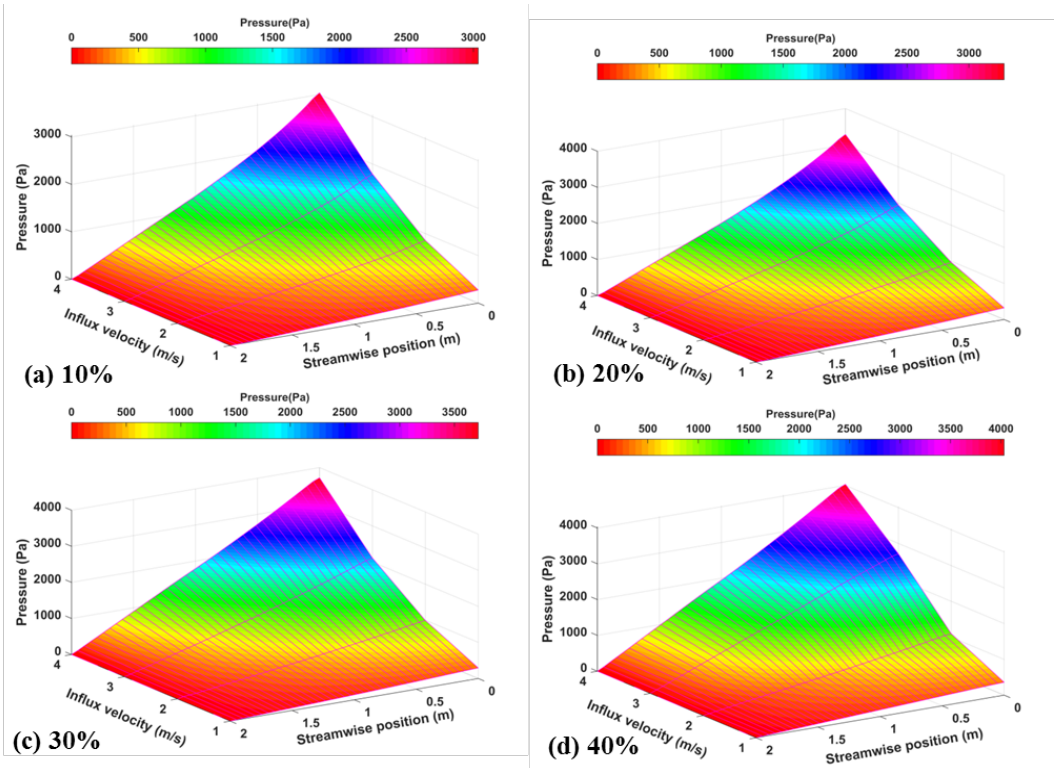

Figure 8. Variation of pressure in streamwise position with (a) 10%, (b) 20%, (c) 30%, and (d) 40% solid concentration for different influx velocities.

The variation of the pressure loss over the whole pipe length is shown in Figure 7 in order to find the length at which the flow has fully developed. It is observed from Figure 7 that there is no appreciable change in pressure loss at a distance of 1m flow from inlet for all slurry concentrations. Therefore, it is concluded that the flow has fully developed after moving a distance of 1m from inlet. This analysis supports the selection of outlet that is 2m apart from the inlet, which is a perfect location for obtaining the results for various flow-related parameters. The similar trends of pressure loss have also been presented by many investigators (Dabirian et al., 2018, Kamyar Najmi et al., 2012, Leporini et al., 2019).

Figure 8 shows variation of the pressure in the whole pipe using all four solid concentrations at all four influx velocities. The pressure in the pipe was measured in Pascal. It is observed from Figure 8 that the pressure intensity is decreasing from inlet to outlet during its flow. It is also observed that the pressure intensity at a point increases with the increase in solid concentration as well as influx velocities.

It is observed from both experimental and numerical analyses that the pressure loss (ΔP) occurs during the sand slurry flow in a horizontal pipe that is a function of slurry concentration (C) and influx velocity (V). A regression analysis has been made to establish the relationship among all parameters affecting the pressure drop. The relationship for experimental data and numerical data obtained separately from regression analysis that is represented in Eq. 6-7, respectively.

$$\Delta P = 9.35C + 542.43V - 716.031 \quad (6)$$

$$\Delta P = 9.31C + 519.68V - 697.9 \quad (7)$$

Granular Pressure Contours

The force exerted on a pipe wall by the solid particles during its motion is called granular pressure. It is also called collisional particle pressure. The granular pressure is measured by calculating the kinetic energy of the oscillating particle motion and their collision. Figures 9a-b show the contours of the granular pressure variation at the outlet of the pipe with all four solid concentrations and all four influx velocities. The granular pressure at the pipe outlet has been measured in Pascal. From Figure 8a, it is observed that the maximum granular pressure is located near the bottom center of the pipe. The present study observed that the granular pressure during transportation of 10% slurry concentration is varying from 2.995e-07 to 8.28e-05 Pa in the variation of velocity of 1–4 m/s. Similarly, the granular pressure during transportation of 40% slurry concentration is varying from 5.692e-03, 3.188e-03, 5.055e-03, and 2.53e-02 Pa in the variation of velocity of 1–4 m/s. It is concluded that the granular pressure is a function of both concentration and influx velocity. It is also observed that the granular pressure is increasing with the increase in both concentration and influx velocity. Since the increase in concentration and velocity increases the momentum transfer and collision during transportation, granular pressure is also expected to increase. Similar results are also obtained by Gopaliya and Kaushal (2015). The granular pressure is also found to possess some value at the upper halves of the wall at higher slurry concentration due to the presence of particles in those regions.

Volume Fraction Contours

The distribution of the particles across the flow domain was investigated by plotting surface contours on a vertical plane in the streamwise direction. The results of this investigation are presented in Figures 10 a-b. It is observed that the volume fraction of solid in the pipe domain during its transportation is a function of velocity and concentration. As the velocity is increased, the turbulence will make the particle always in suspension stage, and therefore, the volume fraction of solid will be more at the middle zone of pipe domain. But at low velocity, the particle will settle during transportation, and the volume fraction will be more at bottom zone of the pipe.

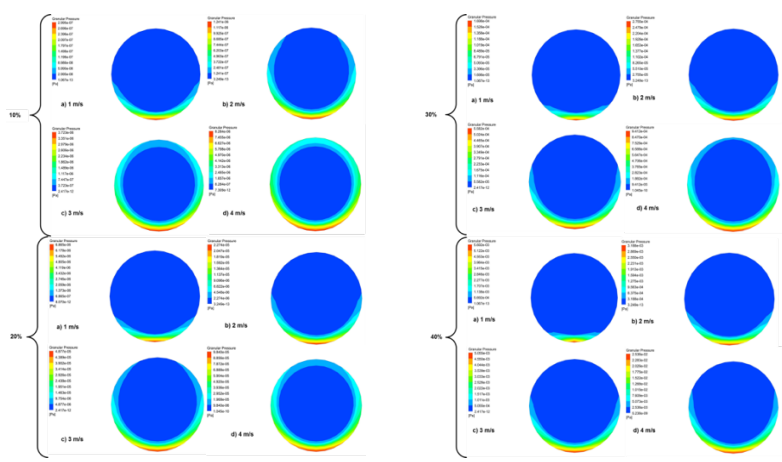

Figure 9. Granular pressure contours at pipe outlet with
a) 10% and 20% b) 30% and 40% solid concentration for 1–4 m/s influx velocity.

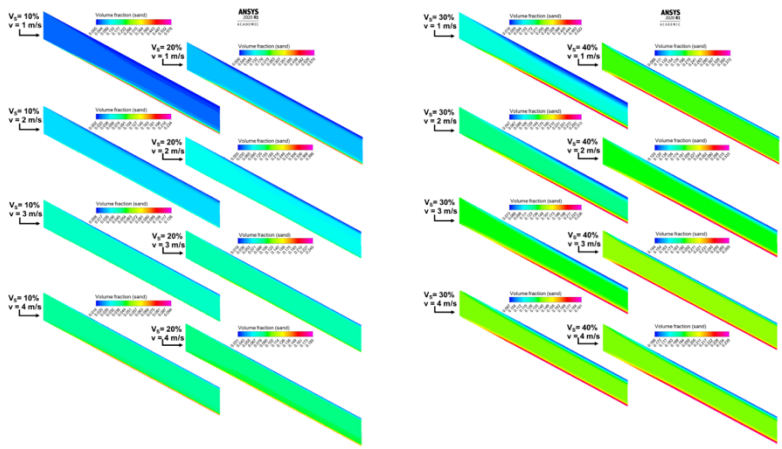

Figure 10. Distribution of particles in the flow domain visualized at a vertical plane in the streamwise direction for (a) slurry concentration 10–20% and (b) slurry concentration 30–40%.

It is observed from Figures 10 a-b that the volume fraction at upper portion of the pipe zone at outlet is 0%, whereas around 25–48% of volume fraction of sand is observed at the bottom zone of outlet for 10–40 % solid concentration and velocity 1-2 m/s. Sine the turbulence generated during flow velocity 1-2 m/s is less, most of the particles got settled during transportation, and therefore, the volume fraction of sand at bottom zone of outlet is increased to 48% when slurry concentration is 10%. During the flow of 40% solid concentration with a velocity of 1-2 m/s, the interaction between particles keeps them in suspension stage, and therefore, a minimum of around 25% of volume fraction of sand is observed at bottom zone of outlet at higher slurry concentration. The increase in velocity (3 and 4 m/s) shows the uniform sand volume concentration at middle zone of the pipe and variation of volume fraction of around 7–20% at bottom zone of the pipe at outlet. Since the turbulence generated during flow velocity 3-4 m/s is more, most of the particles are in suspension stage making most of the pipe domain a uniform solid fraction zone, and therefore, the volume fraction of sand at bottom zone at outlet is observed to decrease to around 7%. The higher concentration at bottom increases when the slurry concentration increases. The similar trends of the volume fraction have also been presented by many investigators (Dabirian et al., 2018, Kamyar Najmi et al., 2012, M.K. singh 2017).

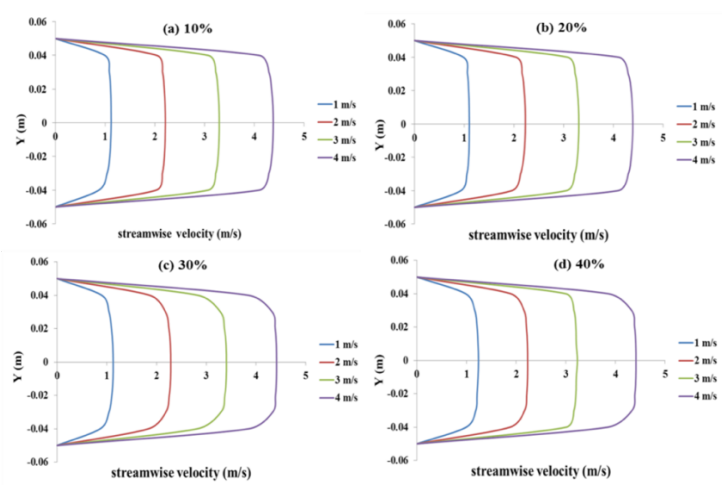

Figure 11. streamwise velocity distributions at (a) 10%, (b) 20%, (c) 30%, and (d) 40% solid concentration.

Slurry Influx Velocity

Figure 11 shows streamwise velocity distribution of sand phase across vertical axis of the pipe outlet for all four solid concentrations with different influx velocities. At low solid concentration and influx velocity, more solid particles settled, and large shear force is observed at the bottom of the pipe, making the velocity distribution profile asymmetrical. However, due to increasing the influx velocity and solid concentration, the velocity distribution profile becomes symmetrical due to the decrease in particle settlement, which reduces the shear force at the bottom zone of pipe. Due to an increase in the influx velocity and solid concentration, the turbulence in the pipe will increase the complete mixing of water and sand particles. It is observed that the velocity distribution profile is symmetrical about the central axis of the pipe. The distribution of the velocity is found to be logarithmic for all cases. Similar trends of the influx velocity have also been presented by many investigators (Archibong-Eso et al., 2020; Vlasak et al., 2020; Sultan et al., 2017; Ekambara et al., 2009).

Skin Friction Coefficient

The skin friction coefficient of the sand phase over the pipe length for all cases is shown in Figure 12. It is observed from Figure 12 that the skin friction coefficient becomes constant when the flow becomes fully developed. Higher skin friction coefficient is observed for lower concentration. It is also seen from Figure 12 that the skin friction coefficient increases with the increase in slurry flow velocity and solid concentration. The similar trends of the skin friction coefficient have also been presented by many researchers (Lin & Ebadian 2008, Ling et al., 2003).

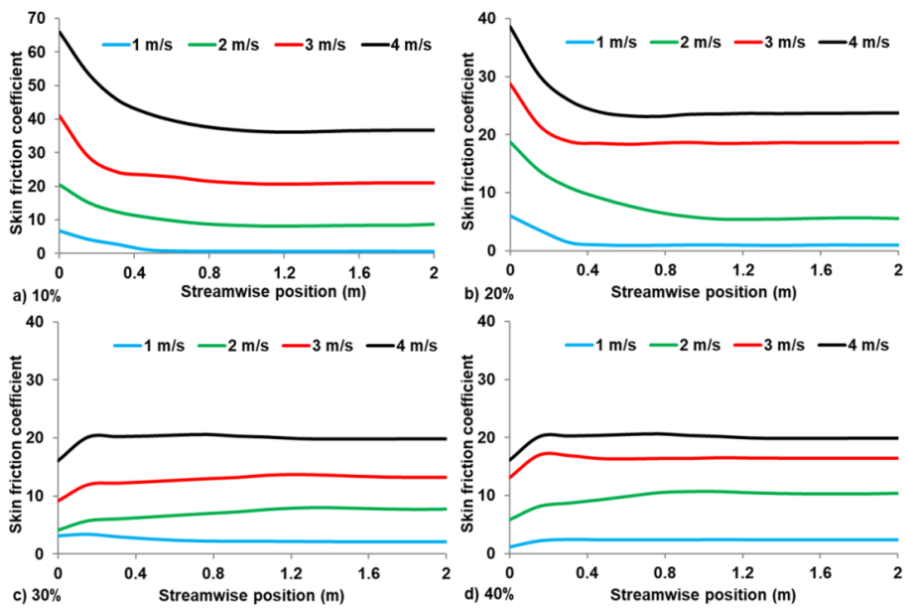

Figure 12. The variation of skin friction coefficient at the pipe wall.
The present graphs represent the average values of the skin friction over the pipe wall.

CONCLUSION

The transportation of sand-water slurry of various concentrations through a horizontal pipeline was investigated both experimentally and numerically. The results obtained through numerical simulation were validated with the experimental results as well as published literature. It is found from the numerical analysis that the solution of governing equations using SST k-omega model provides much accurate results in comparison to other available turbulence models. It is concluded from the analysis of flow characteristics that the pressure loss is a function of slurry concentration and influx velocity. The pressure loss increases as the slurry concentration and influx velocity increase. It is concluded that as the velocity increases four times, the pressure loss in the case of sand slurry flow increases more than 10 times. It is also concluded that the granular pressure is a function of both concentration and influx velocity, and it is increasing with the increase in both concentration and influx velocity. Higher volume fraction of sand at bottom zone of outlet is observed when the slurry concentration and velocity of flow are less, and as both slurry concentration and velocity of flow increase, uniform volume fraction at middle zone of outlet of the pipe is observed. Therefore, the designer should consider the optimum slurry concentration and flow velocity for efficient of sand slurry transportation system.

REFERENCES

Archibong-Eso, A., Aliyu, A. M., Yan, W., Okeke, N. E., Baba, Y. D., Fajemidupe, O., & Yeung, H. (2020). Experimental Study on Sand Transport Characteristics in Horizontal and Inclined Two-Phase Solid-Liquid Pipe Flow. Journal of Pipeline Systems Engineering and Practice, 11(1).

Aude, T., Thompson, T., & Pipelines, E. W. (1975). Slurry pipe line system oil and gas. Journal of Pipeline, 66–67.

Adanez, J., Diego, L.F. de, & Gayan, P. (1993). Transport velocities of coal and sand particles. Powder Technology, 77, 61-68

Ahmed, S. U., Mohanty, S., & Chandra, G. Numerical Analysis of Sand-Water Slurry Flow through Horizontal Pipeline for Various Particle Size at High Velocity.

Dabirian, R., Mohan, R., Shoham, O., & Kouba, G. (2018). Sand Transport in Slightly Upward Inclined Multiphase Flow. Journal of Solar Energy Engineering, Transactions of the ASME, 140(7).

Ekambara, Ak., Sanders, R. S., Nandakumar, K., & Masliyah, J. H. (2009). Hydrodynamic simulation of horizontal slurry pipeline flow using ANSYS-CFX. Industrial and Engineering Chemistry Research, 48(17), 8159–8171.

Ghanta, K. C., & Purohit, N. K. (1999). Pressure drop prediction in hydraulic transport of bi-dispersed particles of coal and copper ore in pipeline. Canadian Journal of Chemical Engineering, 77(1), 127–131.

Gopaliya MK, Kaushal DR. (2015). Analysis of effect of grain size on various parameters of slurry flow through pipeline using CFD. Part Sci Technol, 33(4), 369–84.

Kamyar Najmi, Brenton S. McLaury, and S. A. S. (2012). Low Concentration Sand Transport in Multiphase Viscous Horizontal Pipes: An Experimental Study and Modeling Guideline. AIChE Journal, 62(5), 1821–1833.

Leporini, M., Marchetti, B., Corvaro, F., di Giovine, G., Polonara, F., & Terenzi, A. (2019). Sand transport in multiphase flow mixtures in a horizontal pipeline: An experimental investigation. Petroleum, 5(2), 161–170.

Lin, C. X., & Ebadian, M. A. (2008). A numerical study of developing slurry flow in the entrance region of a horizontal pipe. Computers and Fluids, 37(8), 965–974.

Ling, J., Skudarnov, P. V., Lin, C. X., & Ebadian, M. A. (2003). Numerical investigations of liquid-solid slurry flows in a fully developed turbulent flow region. International Journal of Heat and Fluid Flow, 24(3), 389–398.

Liu, M., Chen, L., & Duan, Y. (2009). Local resistance characteristics of highly concentrated coal-water slurry flow through fittings. Korean Journal of Chemical Engineering, 26(2), 569–575.

Liao, H., Dong, L., Niu, J., Ji, P., Gu, B., & Xu, L. (2020). Study on the Erosion of Screen Pipe Caused by sand-laden slurry. Journal of Engineering Research, 8(4), 258-271.

Menter, F. R. (1994). Two-equation eddy-viscosity turbulence models for engineering applications. AIAA Journal, 32(8), 1598–1605.

Singh, M. K., Kumar, S., Ratha, D., & Sandhu, H. (2019). Improvement in head loss characteristics of fine particulate coalwater suspension with addition of coarser particulate. International Journal of Coal Preparation and Utilization, Accepted.

Sultan, R. A., Rahman, M. A., Rushd, S., & Zendehboudi, S. (2017). CFD simulation of slurry flow in annular pipelines. AIP Conference Proceedings, 1919.

Sundqvist, Å., Sellgren, A., & Addie, G. (1996). Slurry pipeline friction losses for coarse and high density industrial products. Powder Technology, 89(1), 19–28.

Vlasak, P., Matousek, V., Chara, Z., Krupicka, J., Konfrst, J., & Kesely, M. (2020). Concentration distribution and deposition limit of medium-coarse sand-water slurry in inclined pipe. Journal of Hydrology and Hydromechanics, 68(1), 83–91.

Yang, Y., Peng, H., & Wen, C. (2019). Sand transport and deposition behaviour in subsea pipelines for flow assurance. Energies, 12(21).